Sādhanā (2022)47:80
https://doi.org/10.1007/s12046-022-01857-8

Fluid flow and heat transfer in microchannel with and without porous medium under constant heat flux

MOHAMMAD SHAMSODDINI LORI

Department of Mechanical Engineering, Sharif University of Technology, Tehran, Iran
e-mail: m.shams.l7595@gmail.com

MS received 20 October 2021; revised 11 February 2022; accepted 24 February 2022

Abstract. In this study, the heat transfer and fluid flow characteristics of a three-dimensional microchannel that is partially filled with a layer of porous medium at its bottom solid wall is investigated. The microchannel is consisted of a clear fluid flow region, solid walls and a porous layer that is attached to its solid bottom wall. A constant heat flux is applied to the bottom wall of the microchannel. Darcy-Brinkman-Forchheimer model is used to simulate the fluid flow inside the porous medium. The novelty of this work is to investigate thoroughly and precisely the effect of using of porous layer configuration in MCHSs on hydraulic and thermal performances. The effect of porous layer thickness, permeability, porosity, and the mass flow rate on the flow field characteristics and heat transfer performance of the microchannel are examined for the dimensionless porous layer thicknesses $\frac{\delta}{t} = 0, 2, 4, 6, 8,$ and 10. For porous characteristics of $K = 10^{-7}\,\mathrm{m}^2$ and $\varepsilon = 0.6$, the microchannel with dimensionless porous layer thicknesses of $\frac{\delta}{t} = 2$, 4, 6, 8 and 10 have the pressure drop of 1.47, 1.78, 2.11, 2.49, and 2.93 times greater than the microchannel without porous medium respectively. Simultaneously, they have Nusselt number of 1.64, 1.69, 1.75, 1.82 and 1.9 greater than the microchannel without the porous medium respectively. In addition, by increasing of porosity and permeability, the fluid velocity inside the clear region increases, while the fluid velocity inside the porous region decreases, which can be utilized to explain the increase of pressure gradient and Nusselt number.

Keywords. Microchannel; layered porous medium; Nusselt number; pressure drop; Darcy-Brinkman-Forchheimer model.

1. Introduction

For decades, the successful use of microchannels in a wide range of field of studies, such as microfluidics, electronic cooling, medicine, food preparation, and insulation made them an attractive subject for further research [1]. Nowadays, electronic chips become smaller in size and greater in power, which leads to generating huge heat fluxes. Therefore, a proper and small tool, like microchannel, is required to remove those huge amounts of heat.

By the milestone work of Tuckerman and Pease [2], microchannels were introduced to the electronic cooling systems. After that, enhancing the thermos-hydrodynamic productivity, scientists have started to combine microchannels with the other ways of improving the heat transfer and hydrodynamic performances, including using porous medium. In fact, researchers have applied a variety of porous distributions inside the microchannel to ameliorate its productivity, like the porous scaffold [3], wavy porous fins [4] , porous plate [5] and the porous baffles [6].

Steady laminar flow forced convection of a channel with dissimilar porous blocks were studied by Zehforoosh *et al* [7]. Their work leads to 28% reduction in the pressure drop of the channel. Chikh *et al* [8] calculated the friction factor, streamlines, the mean pressure drop, and the dimensionless wall temperature of a channel with porous blocks. Deng *et al* [9] have performed an analytical work for thermally fully developed flow inside a microchannel with porous medium. They calculated the temperature distribution inside the porous substrate. Zhao *et al* [10] have investigated the heat transfer and fluid flow of a microchannel with two approaches of the porous medium and the fins model. They concluded that the increase of channel aspect ratio leads to the increase of overall Nusselt number. Calmidi and Mahajan [11] have studied numerically and experimentally forced convection in high porosity metal foams. They obtained the Nusselt number and other thermal characteristics of various metal foam samples. Chen *et al* [12] have analyzed forced convection in a fluid-saturated porous microchannel. Their main finding is that the fluid inertia force changes drastically the velocity and temperature distribution of the fluid, but has little effect on the solid temperature distribution. Hetsroni *et al* [13] have done experiments to examine the thermal productivity of a

Published online: 16 April 2022

stainless steel sintered porous microchannel. They were successful to remove the heat flux of $6\frac{Mw}{m^2}$ at the pressure drop of 4.5 bar. Lu *et al* [14] have designed a porous fin wavy microchannel to enhance the thermal and hydrodynamic performances at the same time. They decreased the pressure drop and thermal resistance of the porous wavy microchannel compared to the conventional wavy microchannel with solid fins. Xu [15] has accomplished a theoretical research of fully developed forced convection in a microchannel that is centered-filled with porous materials. He studied the impact of Darcy number on the temperature and velocity distribution of the fluid. Hung and Vafai [16, 17] made an improvement in the forced convection heat transfer of a channel with porous block distribution. The nanofluids of TiO_2-water and Al_2O_3-Cu- water were used in a porous wavy microchannel by Elsafy *et al* [18]. They concluded that their design leads to a significant improvement in the thermal outcome of the microchannel. Chuan *et al* [19] have reduced the pressure drop by 49% by developing a porous fin microchannel instead of solid fins. Kozhukhvo *et al* [20] have studied the hydrodynamic performance of an inhomogeneous porous heat exchanger. They compared the results from experimental and mathematical models. Aghamiri *et al* [21] have investigated the forced convection of a two-phase nanofluid flow in a porous microchannel equipping with rotating cylinders. They concluded that the increase of the rotational velocity of the rotating cylinders increases the thermal outcome of the microchannel heat sink. Wang and Li [22] studied analytically the forced convection heat transfer of a bidispere paralleled plate channel under the constant heat flux condition. Their results reveal that the increase of the bidispersivity ends up in a small temperature discrepancy between the wall of the microchannel and the coolant. Li *et al* [23] have represented a theoretical study for the thermal fully developing forced convection in a circular tube filled with porous medium under the local thermal non-equilibrium (LNTE) condition. They concluded that Peclet number, Biot number and the effective thermal conductivity ratio influence strongly the Nusselt number. Xu *et al* [24] have performed a numerical work to examine forced convection of a partially porous filled tube under the LNTE condition. They found that at just the high pore density, the porosity gradient effects the friction factor and Nusselt number. Baragh *et al* [25] have done experiments to investigate heat transfer characteristics of a channel with different porous arrangement. They concluded that the completely porous filled channel has the best heat transfer enhancement for both of the laminar and turbulent flow. Baroon *et al* [26] have presented the heat transfer behavior of a non-Newtonian nanofluid inside a porous medium. They found that the increase of the porous layer influences the thermal performance much greater than the Reynolds number does. The heat transfer field and fluid flow characteristics of microchannel heat sinks with miscellaneous structures of metal foams is investigated by Shen *et al* [27]. They identified that the combined design of the Y-shaped and fin structures metal foams has the best overall heat transfer performance. Sheremet *et al* [28] have studied the unsteady natural convection in a partially porous filled vertical cylinder. They discussed the effect of major factors, like Darcy number, porous layer height ratio, and the solid wall thickness on the key parameters like Nusselt number and the average temperature in a cavity. Mahmoudi [29] has investigated the heat transfer of a microchannel that is filled with porous medium with the internal heat generation for two primary approaches models. He obtained the average Nusselt number and friction factor for those two models. Hung *et al* [30] have tested miscellaneous porous configurations in a microchannel heat sink. Their findings divulged that the trapezoidal and sandwich distribution have the best thermal and hydraulic performance, respectively. Yang *et al* [31] have calculated the pressure drop and average Nusselt number for the turbulent flow in a porous-baffled microchannel. They documented that the increase of the baffle height leads to improve the thermal productivity of the microchannel.

Even though in the earlier mentioned studies, researchers have investigated the average Nusselt number and pressure drop of porous MCHSs, and most of these works just compared different porous configurations to one another, but it is essential to thoroughly and precisely examine the effect of the porous layer thickness on the hydraulic and thermal behaviors of MCHSs with the porous layer configuration (one of most effective configuration in both thermal and hydraulic performances). Therefore, the objective of this work is to delve in the effect of porous layer thickness on the performance of MCHS. Particularly, the hydraulic and thermal parameters, including pressure along the channel, velocity profiles in different directions, pressure drop, averaged Nusselt number and local Nusselt number were assessed in depth. In addition, the effect of porous characteristics- permeability and porosity, and mass flow rate were evaluated on the previous mentioned heat transfer and hydraulic parameters. We perform a numerical analysis of the forced convection heat transfer within a microchannel that is partially filled with different thicknesses of the porous layered distribution using Darcy-Brinkman-Forchheimer model to simulate the fluid flow transport inside the porous medium.

2. Problem description and methods

2.1 *Computational domain*

To perform this numerical work, a single microchannel with vertical solid walls and a porous layer that is attached to its bottom solid wall is chosen. Figure 1 shows the chosen microchannel, the computational domains, solid

walls, a constant heat flux at the bottom, and geometric parameters. The microchannel is with the length (L), width (w), height (H) and the solid thickness (t) of 10 mm, 0.8 mm, 2.5 mm, and 0.1 mm, respectively. The studied dimensionless porous layer thicknesses are $\frac{\delta}{t} = 0, 2, 4, 6, 8$ and 10. For a better assessing of the performance of examined designs, a conventional microchannel without porous medium is selected.

2.2 *Formulation and governing equations*

A three-dimensional model is developed to simulate the heat transfer and fluid flow of a partially filled porous microchannel. The continuity, momentum, and energy equations are solved simultaneously in the clear region and the porous region, which is assumed to be non-deformable, homogeneous, and isotropic [30]. The fluid flow is laminar and incompressible, flow and heat transfer are in steady-state condition and thermosphysical properties are not changing in working temperatures. Local thermal equilibrium (LTE) condition is conjectured between the solid and liquid phases of the porous medium [16, 17, 30]. For the simulation of fluid flow through the clear region, we use the Navier-Stokes equation (equation 3), and through the porous region, the Darcy-Brinkman-Forchheimer equation is used (equation 4, Darcy-Forchheimer terms are added; the first term $-\frac{\mu_f}{K}\overrightarrow{V}$ is the famous Darcy law that links linearly the pressure drop and flow velocity in a porous medium. This term is added because of pressure drop effectuated by frictional drag. At higher velocities and heat transfer point of view, the inertial effects become more significant, and it required adding the second term $-\frac{\rho_f C}{\sqrt{K}}\left|\overrightarrow{V}\right|\overrightarrow{V}$ to the momentum equations to account for the form drag; in fact, in high porosity $\varepsilon \cong 1$, and very high permeability these two terms approach to Zero and the momentum equations approach to the standard Navier-Stokes equations (momentum equations of the free flow region)) [32–34]. Also, we use equations (5) and (6) for simulation heat transfer in the clear and porous regions respectively. The velocity field $\overrightarrow{V}$, temperature T, and pressure p are not changing at the interface between the clear region and the porous region ($\overrightarrow{V_e} = \overrightarrow{V_f}$, $p_e = p_f$ and $T_e = T_f$), these fields are the same for both regions. Contrary, the heat flux and stress are not continuous at the interface [34–39]. More details about the boundary conditions and equations at the interface between the clear region and porous medium can be seen in these references [33, 38]. Based on the aforementioned speculations, the continuity, momentum and energy equations are:

Continuity for the clear region:

$$\frac{\partial(\rho_f u_f)}{\partial x} + \frac{\partial(\rho_f v_f)}{\partial y} + \frac{\partial(\rho_f w_f)}{\partial z} = 0 \tag{1}$$

Continuity for the porous layer:

$$\frac{\partial(\rho_f \varepsilon u_e)}{\partial x} + \frac{\partial(\rho_f \varepsilon v_e)}{\partial y} + \frac{\partial(\rho_f \varepsilon w_e)}{\partial z} = 0 \tag{2}$$

Momentum equations in the clear region:

$$\begin{aligned}
&\rho_f\left(u_f\frac{\partial u_f}{\partial x} + v_f\frac{\partial u_f}{\partial y} + w_f\frac{\partial u_f}{\partial z}\right)\\
&\quad = -\frac{\partial p_f}{\partial x} + \mu_f\left(\frac{\partial^2 u_f}{\partial x^2} + \frac{\partial^2 u_f}{\partial y^2} + \frac{\partial^2 u_f}{\partial z^2}\right)\\
&\rho_f\left(u_f\frac{\partial v_f}{\partial x} + v_f\frac{\partial v_f}{\partial y} + w_f\frac{\partial v_f}{\partial z}\right)\\
&\quad = -\frac{\partial p_f}{\partial y} + \mu_f\left(\frac{\partial^2 v_f}{\partial x^2} + \frac{\partial^2 v_f}{\partial y^2} + \frac{\partial^2 v_f}{\partial z^2}\right)\\
&\rho_f\left(u_f\frac{\partial w_f}{\partial x} + v_f\frac{\partial w_f}{\partial y} + w_f\frac{\partial w_f}{\partial z}\right)\\
&\quad = -\frac{\partial p_f}{\partial z} + \mu_f\left(\frac{\partial^2 w_f}{\partial x^2} + \frac{\partial^2 w_f}{\partial y^2} + \frac{\partial^2 w_f}{\partial z^2}\right)
\end{aligned} \tag{3}$$

Momentum equations in the porous region:

$$\begin{aligned}
&\frac{\rho_f}{\varepsilon^2}\left(u_e\frac{\partial u_e}{\partial x} + v_e\frac{\partial u_e}{\partial y} + w_e\frac{\partial u_e}{\partial z}\right)\\
&\quad = -\frac{\partial p_e}{\partial x} + \frac{\mu_f}{\varepsilon}\left(\frac{\partial^2 u_e}{\partial x^2} + \frac{\partial^2 u_e}{\partial y^2} + \frac{\partial^2 u_e}{\partial z^2}\right)\\
&\qquad - \frac{\mu_f}{K}u_e - \frac{\rho_f C}{\sqrt{K}}\left|\overrightarrow{V_e}\right|u_e\\
&\frac{\rho_f}{\varepsilon^2}\left(u_e\frac{\partial v_e}{\partial x} + v_e\frac{\partial v_e}{\partial y} + w_e\frac{\partial v_e}{\partial z}\right)\\
&\quad = -\frac{\partial p_e}{\partial y} + \frac{\mu_f}{\varepsilon}\left(\frac{\partial^2 v_e}{\partial x^2} + \frac{\partial^2 v_e}{\partial y^2} + \frac{\partial^2 v_e}{\partial z^2}\right)\\
&\qquad - \frac{\mu_f}{K}v_e - \frac{\rho_f C}{\sqrt{K}}\left|\overrightarrow{V_e}\right|v_e\\
&\frac{\rho_f}{\varepsilon^2}\left(u_e\frac{\partial w_e}{\partial x} + v_e\frac{\partial w_e}{\partial y} + w_e\frac{\partial w_e}{\partial z}\right)\\
&\quad = -\frac{\partial p_e}{\partial z} + \frac{\mu_f}{\varepsilon}\left(\frac{\partial^2 w_e}{\partial x^2} + \frac{\partial^2 w_e}{\partial y^2} + \frac{\partial^2 w_e}{\partial z^2}\right)\\
&\qquad - \frac{\mu_f}{K}w_e - \frac{\rho_f C}{\sqrt{K}}\left|\overrightarrow{V_e}\right|w_e
\end{aligned} \tag{4}$$

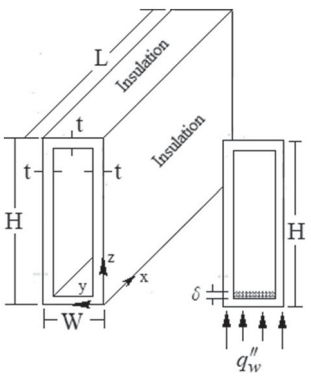

Figure 1. Schematic of the microchannel with a porous layer on the bottom.

Where $\left|\overrightarrow{V_e}\right| = \sqrt{{u_e}^2 + {v_e}^2 + {w_e}^2}$

Energy equation in the clear region:

$$\rho_f\left(u_f\frac{\partial T_f}{\partial x} + v_f\frac{\partial T_f}{\partial y} + w_f\frac{\partial T_f}{\partial z}\right) = \frac{k_f}{c_{pf}}\left(\frac{\partial^2 T_f}{\partial x^2} + \frac{\partial^2 T_f}{\partial y^2} + \frac{\partial^2 T_f}{\partial z^2}\right) \tag{5}$$

Energy equation in the porous region:

$$\begin{aligned}(\rho c_p)_e\left(u_e\frac{\partial T_e}{\partial x} + v_e\frac{\partial T_e}{\partial y} + w_e\frac{\partial T_e}{\partial z}\right)\\ = k_e\left(\frac{\partial^2 T_e}{\partial x^2} + \frac{\partial^2 T_e}{\partial y^2} + \frac{\partial^2 T_e}{\partial z^2}\right)\end{aligned} \tag{6}$$

Energy equation of solid walls:

$$k_w\left(\frac{\partial T_w}{\partial x} + \frac{\partial T_w}{\partial y} + \frac{\partial T_w}{\partial z}\right) = 0 \tag{7}$$

u, v, and w are the velocities in x, y, and z direction respectively. p is the fluid pressure, T is the temperature, μ is the dynamic viscosity, k is the thermal conductivity, c_p is the specific heat capacity, ε is porosity of the porous medium, K is permeability, C is Forchheimer's constant ($C = \frac{1.75\varepsilon^{-3/2}}{\sqrt{150}}$). The effective heat capacity and thermal conductivity of porous layer are $(\rho c_p)_e = \varepsilon\rho_f c_{pf} + (1-\varepsilon)\rho_s c_s$ and $k_e = \varepsilon k_f + (1-\varepsilon)k_s$. Indexes *f*, *s*, *e*, and *w* refer to the fluid, solid, porous region, and walls.

2.3 *Boundary conditions*

For microchannel without porous medium

Channel Inlet:

$$\begin{aligned}&u_f(0, t<y<w-t, t<z<H-t)\\ &= u_{in}, T_f(0, t<y<w-t, t<z<H-t) = T_{in},\\ &\frac{\partial T_w}{\partial x}(0, 0<y<t \& w-t<y<w, 0<z<t \& H-t<z<H)\\ &= 0\end{aligned}$$

Channel outlet

$$\begin{aligned}&p_f(L, t<y<w-t, t<z<H-t)\\ &= p_{out}, \frac{\partial T_f}{\partial x}(L, t<y<w-t, t<z<H-t) = 0\\ &\frac{\partial T_w}{\partial x}(L, 0<y<t \& w-t<y<w, 0<z<t \& H-t<z<H)\\ &= 0\end{aligned}$$

Inner bottom wall of the microchannel $z(x,\ t<y<w-t,\ t)$:

$$u_f = v_f = w_f = 0, -k_w\frac{\partial T_w}{\partial z} = -k_f\frac{\partial T_f}{\partial z}, T_f = T_w$$

Bottom surface $z(x, y, 0)$:

$$-k_w\frac{\partial T_w}{\partial z} = q_w$$

Inner top wall of the microchannel $z(x, t<y<w-t, H-t)$:

$$u_f = v_f = w_f = 0, -k_f\frac{\partial T_f}{\partial z} = -k_w\frac{\partial T_w}{\partial z}, T_f = T_w$$

Inner side surfaces $y(x, t, t<z<H-t)$ and $y(x, w-t, t<z<H-t)$:

$$u_f = v_f = w_f = 0, -k_w\frac{\partial T_w}{\partial y} = -k_f\frac{\partial T_f}{\partial y}, T_f = T_w$$

Other surfaces are kept insulated:

$$\frac{\partial T_w}{\partial y}(x, 0, z) = \frac{\partial T_w}{\partial y}(x, w, z) = \frac{\partial T_w}{\partial z}(x, y, H) = 0$$

For the microchannel with porous medium

Channel inlet:

$$\begin{aligned}&u_f(0,\ t<y<w-t,\ t+\delta<z<H-t)\\ &= u_e(0,\ t<y<w-t,\ t<z<t+\delta) = u_{in},\\ &T_f(0,\ t<y<w-t,\ t+\delta<z<H-t)\\ &= T_e(0,\ t<y<w-t,\ t<z<t+\delta) = T_{in},\\ &\frac{\partial T_w}{\partial x}(0, 0<y<t \ \&\ w-t<y<w,\\ &0<z<t \ \&\ H-t<z<H) = 0\end{aligned}$$

Channel outlet:

$$\begin{aligned}&p_f(L,\ t<y<w-t,\ t+\delta<z<H-t)\\ &= p_e(L,\ t<y<w-t,\ t<z<t+\delta) = p_{out},\\ &\frac{\partial T_w}{\partial x}(L, 0<y<t \ \text{and}\ w-t<y<w,\\ &0<z<t \ \text{and}\ H-t<z<H)\\ &= \frac{\partial T_f}{\partial x}(L,\ t<y<w-t,\ t+\delta<z<H-t)\\ &= \frac{\partial T_e}{\partial x}(L,\ t<y<w-t,\ t<z<t+\delta) = 0\end{aligned}$$

Inner bottom wall of the microchannel (between the bottom solid wall and the porous region)

$$\begin{aligned}Z(x,\ t<y<w-t,\ t):\quad &u_e = v_e = w_e = 0,\\ -k_w\frac{\partial T_w}{\partial z} &= -k_e\frac{\partial T_e}{\partial z}, \quad T_w = T_e\end{aligned}$$

Bottom surface

$$z\ (x,\ y,\ 0) : -k_w\frac{\partial T_w}{\partial z} = q_w$$

Surface between the porous region and clear region

$$Z(x,\ t<y<w-t, t+\delta): \quad -k_e\frac{\partial T_e}{\partial z} = -k_f\frac{\partial T_f}{\partial z},$$
$$u_e = u_f, \quad v_e = v_f, \quad w_e = w_f, \quad T_e = T_f$$

Inner top wall of the microchannel

$$Z(x,\ t<y<w-t,\ H-t): \quad u_f = v_f = w_f = 0,$$
$$-k_w\frac{\partial T_w}{\partial z} = -k_f\frac{\partial T_f}{\partial z}, \quad T_w = T_f$$

Inner side surfaces

$$y(x,\ w-t,\ z): u = v = w = 0,$$
$$\left[-k_w\frac{\partial T_w}{\partial y} = -k_f\frac{\partial T_f}{\partial y} \text{ and } T_w = T_f\right]_{H-t>z>t+\delta},$$
$$\left[-k_w\frac{\partial T_w}{\partial y} = -k_e\frac{\partial T_e}{\partial y} \text{ and } T_w = T_e\right]_{t\le z\le t+\delta}$$

The inlet velocity is $u_{in} = \frac{1m}{s}$ and the inlet temperature is $T_{in} = 300$ K. The constant heat flux is 100 W/cm^2. The working fluid is water, and the solid walls and porous medium are made of stainless steel. The thermosphysical properties are shown in table 1.

2.4 *Data reduction*

To determine the fluid flow and heat transfer characteristics inside the microchannel some parameters of interest are defined as below

The Reynolds number

$$Re = \frac{\rho_f u_m D_h}{\mu_f} \tag{8}$$

The friction factor

$$f = \frac{(p_{in}-p_{out})2D_h}{\rho_f L u_m{}^2} \tag{9}$$

The Nusselt number

$$Nu = \frac{q_w D_h}{(T_w - T_{in})k_f} \tag{10}$$

Where ρ_f is the fluid density, μ_f is the fluid dynamic viscosity, p_{in} *and* p_{out} are the pressure at the inlet and outlet of the microchannel, L is the length of the microchannel, u_m is the average velocity of the fluid along the channel, T_{in} is the inlet temperature, q_w is the constant heat flux, $D_h = \frac{2(H-2\times t)(W-2\times t)}{(H-2\times t)+(W-2\times t)}$ is the hydraulic diameter, k_f is the fluid thermal conductivity. In the equation (10), T_w is the temperature along the centerline of the bottom surface, and this consideration is based on previous published works [16, 30, 40–42]. In these studies, the thermal conductivity of fluid k_f is also used to define the Nusselt number.

3. Numerical procedure

In both industry and nature, there are systems that fluid flows in a clear domain and porous medium at the same time, like flowing of water atop and inside of mushy layers [43, 44]. However, one approach to simulate the above-mentioned systems is utilizing Navier-Stokes equations in the clear region and Darcy equation in the porous region [45, 46]. Darcy-Brinkman-Forchheimer equation is widely utilized to simulate the fluid transport through the porous regions. The main problem with the simultaneous pure flow and porous flow domains is the boundary condition that is considered between those two domains. This boundary condition has been studied in a great deal of experimental and analytical works. Beavers and Joseph [36] have performed an experimental work to repudiate the accuracy of previous considered boundary conditions at the interface between the clear flow region and porous medium, and they proposed a discontinuity in the interfacial tangential velocity as below

$$u_s - u_D = \frac{\sqrt{K}}{\beta}\frac{\partial u_s}{\partial z} \tag{11}$$

Where u_s is the fluid velocity of clear region calculated by Stokes equations, u_D is the fluid velocity of porous medium calculated by Darcy equation, K is permeability, z is perpendicular to the interface between the clear flow region and the porous medium and β is a dimensionless coefficient that depends on the structure of the porous medium and the pure fluid domain. Ochoa-Tapia and Whitaker [47, 48] proposed a continuity of the tangential velocity and discontinuity of the tangential shear stress. Nader and Neale [49] considered continuity of both the tangential velocity and tangential shear stress. Cieszko and Kubik [50] used discontinuity of both the tangential

Table 1. Thermosphysical properties of the fluid, the solid section, and the porous medium.

Materials	ρ (kg m^{-3})	c_p (J kg^{-1} K^{-1})	k (W m^{-1} K^{-1})	μ (kg m^{-1} s^{-1})
Working fluid: Pure water	998.2	4182	0.6	0.000885
Solid section: Stainless steel	8000	500	16.7	
Porous layer: Stainless steel	8000	500	16.7	

velocity and tangential shear stress. However, in this work, the fluid velocity and pressure in the clear flow region and porous medium is assumed to be continuous over the interface between the free flow and the porous medium.

Various thicknesses of a porous layer are placed in a three-dimensional microchannel, and governing equations are numerically solved simultaneously using COMSOL Multiphysics. The finite element method (FEM) is used for this numerical model. The solver uses generalized minimal residual method (GMRES) as an iterative method for the numerical solution. Discretization of P2+P1, second order elements for the velocity and temperature components, and a linear for the pressure components, is used for governing equations. To set the results free from elements size, five different element numbers are utilized to calculate the maximum wall temperature and pressure drop of the microchannel with porous layer thickness of $\frac{\delta}{t}$=4 and porous characteristics of $\varepsilon = 0.6$ and $K = 10^{-7}$, shown in table 2. As can be seen, between the number elements of 1.575 million and 1.882 million, there is not an obvious discrepancy for the results, therefore, the element numbers of 1.575 million is chosen. The considered relative tolerance is 10^{-5}. Relative tolerance is a criterion for termination of computation based on the Residual and Solution relative error that are calculated as the weight Euclidean norm [35, 51]. In fact, when the Residual and Solution relative error exceed the considered relative tolerance, the computation will be stopped. To validate the present numerical model, some previous experimental, numerical and theoretical works are selected. In this regard, in figure 2, the friction factor versus Reynolds number is calculated by the theoretical correlation (equations (12) and (13)) [52], the experimental work of Jung *et al* [53] and the present numerical model for the microchannel with rectangular cross-section with dimensions of 100 µm × 100 µm × 15 mm and working fluid of water. There are several reasons that leads to deviating of the numerically calculated friction factor from the experimental and theoretical ones, such as uncertainty in experimental tools, like pressure gage and gas sources regulator; and the friction pressure drop in the manifold was neglected. Also, we assumed that the fluid reaches the fully developed condition at the beginning of the microchannel and it happens earlier than the fluid does in the experiment. Numerical and experimental data usually deviate from each other because of involved errors in numerical algorithms.

Table 2. Mesh independency study for a microchannel with dimensionless porous layer of $\frac{\delta}{t} = 4$.

Number of cells (million)	$T_{w,max}$(K)	Δp(kPa)
0.15	360.63	592.7
0.485	362.56	602.1
0.955	363.21	608
1.575	364	612
1.882	364.05	612.78

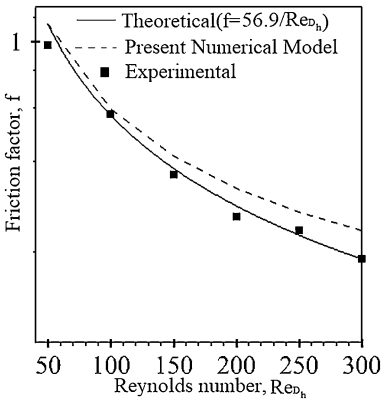

Figure 2. Friction factors depending on Reynolds numbers of rectangular microchannel with aspect ratio of $\alpha = 1$, for the theoretical correlation [52], the experimental work of Jung *et al* [53] and the present numerical model.

$$f_{Lam} = \frac{96}{Re_{Dh}}(1 - 1.3553\alpha + 1.9467\alpha^2 - 1.7012\alpha^3 + 0.9564\alpha^4 - 0.2537\alpha^5) \quad (12)$$

Where α is aspect ratio and for $\alpha = 1$, we have

$$f = \frac{56.9}{Re_{Dh}} \quad (13)$$

In addition, the Nusselt number for developed flow inside a rectangular microchannel is calculated by the present numerical model and compared to a previous theoretical published work. For the fully developed flow, a correlation of the Nusselt number is proposed by Shah and London [52].

$$Nu_{fd} = 8.235(1 - 2.0421\alpha + 3.0853\alpha^2 - 2.4765\alpha^3 + 1.0578\alpha^4 - 0.1861\alpha^5) \quad (14)$$

At first, in figure 3, the fully developed Nusselt number versus the aspect ratio (with the range of $\alpha = 0.1 - 1$) for a rectangular microchannel with fully developed flow is calculated by the present model and compared with the aforementioned theoretical correlation (equation (14)) of fully developed Nusselt number.

Further, for the fully developing flow, the local Nusselt number (Nu_x) versus the dimensionless axial distance $(x^* = \frac{x/D_h}{RePr})$ of a microchannel with rectangular cross-section under constant heat flux for Reynolds number of Re=400 is presented by this study and compared with the numerical study of Ma *et al* [54] shown in figure 4. The local Nusselt number for the comparison work [54] (figure 4) is calculated by $Nu_x = h_x D_h/k$ and $h_x = q_w/(T_{w,x} - T_{m,x})$, where q_w is the heat flux applied the bottom surface, $T_{w,x}$ is the temperature alongside the bottom surface, and $T_{m,x}$ is the

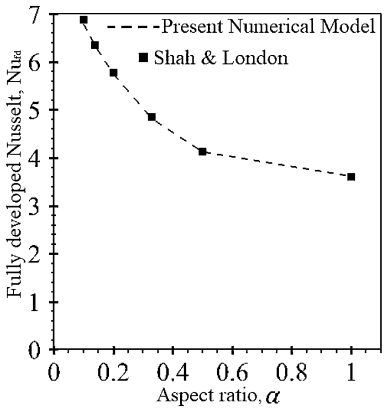

Figure 3. Comparison of the present numerical model with the theoretical correlation of Shah and London [52] of fully developed Nusselt number versus aspect ratio for the rectangular microchannel with working fluid of water.

mean temperature of the fluid along the microchannel [54]. Nusselt number of the fully developed region (figure 3) is calculated by the wall temperature at approximately end of the microchannel, where we assure to reach to the fully developed region [54, 55]. As can be noticed, in all these comparison works, the results have an excellent agreement with one another and the maximum discrepancy is less than ±0.5%.

4. Result and discussion

For this work, the effect of the porous layer thickness, porous characteristics of porosity and permeability and mass flow rate on the heat transfer and fluid flow features of a partially porous filled microchannel are investigated. The different porous layer thicknesses are $\frac{\delta}{t} = 0, 2, 4, 6,$ 8 and 10. Porosity is $\varepsilon = 0.4$ and 0.6. Permeability is $K = 10^{-7}\text{m}^2$ and 10^{-9}m^2. The microchannel without the

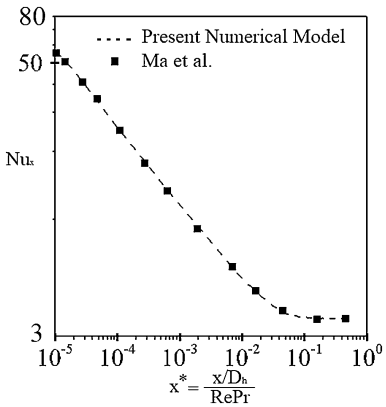

Figure 4. Comparison of the local Nusselt number Nu_x with the numerical result of Ma *et al* [54] Re = 400, $Pr = 7$.

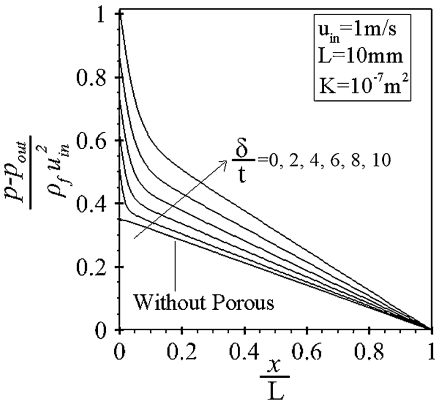

Figure 5. Effect of the porous layer thickness on the pressure gradient along the partially porous filled microchannel for porosity $\varepsilon = 0.6$.

porous medium is also selected as the reference for comparison.

Figure 5 shows the effect of the porous layer thickness on the pressure gradient along the microchannel with porosity of $\varepsilon = 0.6$ and permeability of $K = 10^{-7}\text{m}^2$. The pressure gradient along the microchannel has been dimensionless by the inlet fluid velocity. The pressure gradient of the microchannel without a porous medium is also represented for comparison. As can be seen, microchannels with porous medium have significantly larger dimensionless pressure gradient compared to the non-porous microchannel, especially at the begging of the microchannel. By increasing of the porous layer thickness, the pressure gradient along the microchannel increases, and this increase is more significant for higher porous layer thicknesses. This is because with the increase in porous layer thickness, the area of flow inside the clear media gets reduced. The average flow velocity inside the porous region is smaller and hence in order to conserve mass the average flow velocity in the clear region is larger.

Figure 6 illustrates the effect of porosity and permeability on the dimensionless pressure gradient between the outlet and inlet cross section of the microchannel versus the porous layer thickness. Reducing of porosity and permeability results in an increase in the pressure gradient. In fact, reduction of permeability from $10^{-7}\,\text{m}^2$ to $10^{-9}\,\text{m}^2$ leads to 260% augment in the pressure drop on average; while reduction of porosity from $\varepsilon = 0.6$ to $\varepsilon = 0.4$ leads to the pressure drop increases by just 28%. This is because the porous medium with lower permeability and porosity resists more against the fluid flow and provides more blockage forces that prevent fluid from flowing. It can be known that, the decrease of permeability has much more influence on the pressure drop than porosity does.

The variations of the pressure drop $\Delta p = p_{in} - p_{out}$ between the inlet and outlet cross section of the partially porous filled microchannel with miscellaneous porous layer thicknesses versus the mass flow rate is exhibited in

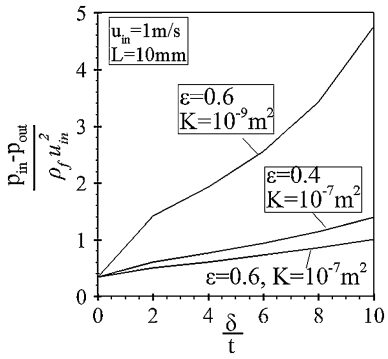

Figure 6. Effect of porosity and permeability on the pressure gradient at the inlet and outlet of the microchannel versus the porous layer thickness.

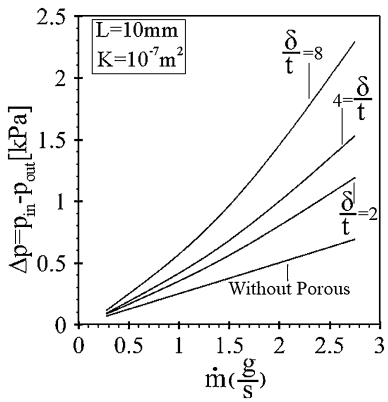

Figure 7. The variation of pressure drop versus the mass flow rate for non-porous microchannel and partially porous filled microchannel with various porous layer thicknesses.

figure 7. Porosity is $\varepsilon = 0.6$ and permeability is $K = 10^{-7}\,\mathrm{m}^2$. The effect of mass flow rate on the pressure drop of microchannel without porous medium is also shown. By increasing the mass flow rate, the pressure drop of both the microchannel with and without porous medium increases, and the rate of this increase is larger for the partially porous filled microchannel compared to the non-porous microchannel. By increasing the porous layer thickness, the pressure drop increases more rapidly with the increase of mass flow rate.

Figure 8 depicts the effect of the porous layer thickness on the x-direction fully developed velocity profile of the microchannel with porosity of $\varepsilon = 0.6$, permeability of $K = 10^{-7}\,\mathrm{m}^2$ and inlet velocity of $u_{in} = \frac{1\mathrm{m}}{\mathrm{s}}$. This figure indicates the fully developed velocity profile for six miscellaneous dimensionless porous layer thicknesses of $\frac{\delta}{t} = 0, 2, 4, 6, 8,$ and 10. The velocity profile in the clear region is a laminar flow and in the porous region is a Darcy flow with a uniform distribution. With the increase of porous layer thickness, the fluid velocity in the clear region increases,

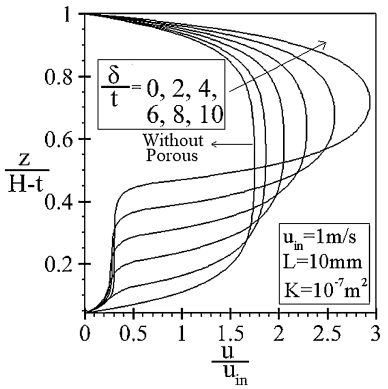

Figure 8. Effect of the porous layer thickness on the x-direction fully developed velocity of the microchannel for porosity of ε = 0.6.

and the velocity profile's peak with the maximum velocity moves toward the microchannel's top solid wall. For example, with the increase of porous layer thickness from $\frac{\delta}{t} = 4$ to $\frac{\delta}{t} = 8$, the maximum velocity changes from $\frac{u}{u_{in}} = 2.05$ at $\frac{z}{H-t} = 0.59$ to $\frac{u}{u_{in}} = 2.57$ at $\frac{z}{H-t} = 0.677$. The fully developed velocity profile of the microchannel without porous medium is also shown ($\frac{\delta}{t} = 0$). With vanishing of the porous layer, the clear flow region with a laminar flow regime occupied the entire microchannel with the maximum velocity of $\frac{u}{u_{in}} = 1.75$. At higher porous layer thicknesses, the influence of the porous layer thickness on the fully developed velocity profile become more obvious.

Figure 8 is reproduced in figure 9 for two dimensionless porous layer thicknesses of $\frac{\delta}{t} = 4$ and $\frac{\delta}{t} = 8$ to examine the effect of porosity and permeability on the x-direction fully developed velocity profile. It can be noticed that the shape of fully developed velocity profile is the same for different porosity and permeability values. As permeability and porosity declines, the fluid velocity inside the porous region decreases, and the fluid velocity inside the clear region increases. For example, with reducing permeability from $K = 10^{-7}\,\mathrm{m}^2$ to $K = 10^{-9}\,\mathrm{m}^2$, for microchannel with the dimensionless porous layer thickness of $\frac{\delta}{t} = 8$, the dimensionless fluid velocity inside the porous region changes from 0.3 to 0.1; and the maximum velocity in the clear region changes from 2.57 to 2.78. In fact, the decline of permeability and porosity makes the porous medium resists more against the fluid flow. It can be also discerned that at the higher porous layer thickness, the change of permeability and porosity has more effect of the fully developed fluid velocity profile.

Figure 10 displays the z-direction fluid velocity profile for microchannels with various porous layer thicknesses at $x = 0.35\,\mathrm{mm}$. Porosity is $\varepsilon = 0.6$, permeability is $K = 10^{-7}\,\mathrm{m}^2$ and the inlet velocity is $u_{in} = \frac{1\mathrm{m}}{\mathrm{s}}$. With increasing the porous layer thickness the fluid velocity in z-direction increases in the clear region and decreases in the porous

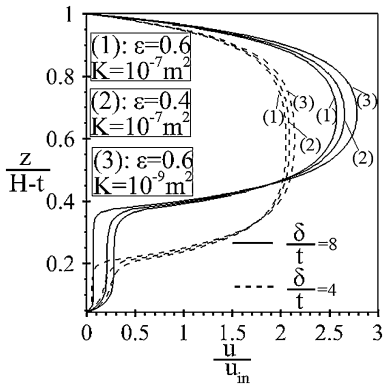

Figure 9. Effect of porosity and permeability on the x-direction fully developed velocity for two different dimensionless porous layer thickness of $\frac{\delta}{t} = 4$ and $\frac{\delta}{t} = 8$; inlet velocity is $u_{in} = \frac{1m}{s}$.

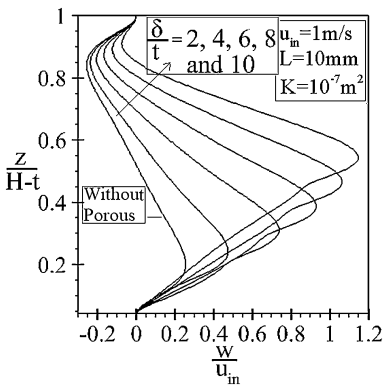

Figure 10. z-direction fluid velocity profile for the microchannel with various porous layer thickness at $x = 0.35$ mm and $\varepsilon = 0.6$.

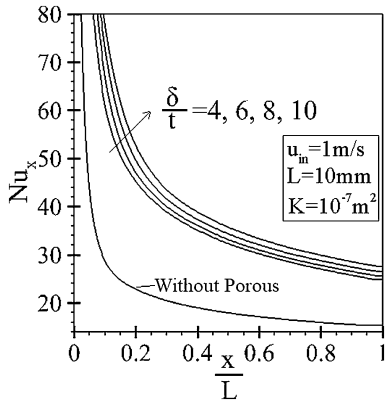

Figure 11. Effect of the porous layer thickness on the local Nusselt number along the microchannel, ε = 0.6.

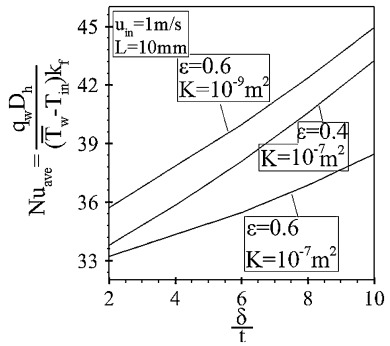

Figure 12. Effect of porosity and permeability on the average Nusselt number Nu_{ave} of microchannels versus the porous layer thickness.

region. In fact, with the increase of porous layer thickness, more hot fluid in the porous region come in the clear flow region with the cold fluid, resulting in a better convective heat transfer by the coolant.

Figure 11 depicts the effect of porous layer thickness on the local Nusselt number Nu_x along the microchannel with porosity of ε = 0.6 and permeability of $K = 10^{-7}$ m^2. After a short thermal entrance length, microchannels with various porous layer thicknesses approach to their fully developed thermal conditions with a constant value of the Nusselt number. In fact, the increase of porous layer thickness leads to the increase of thermal entrance length. By increasing of the porous layer thickness, the heat transfer performance of the microchannel improves, gaining higher local Nusselt number. This improvement can be elucidated by the fact that with increasing porous layer thickness, more hot fluid is forced from the porous medium toward the clear region with the cold fluid, better mixture of the hot fluid in the porous region and cold fluid in the clear region is obtained. In addition, the hydrodynamic boundary layer thickness become thinner next to the wall and more momentum and energy fluxes can be exchanged there due to the higher velocity of fluid.

Figure 12 shows the impact of porosity and permeability on the average Nusselt number Nu_{ave} versus the porous layer thickness. The inlet velocity is $u_{in} = 1\frac{m}{s}$ and the constant heat flux that is applied to the bottom wall of microchannel is $q_w = 100\frac{W}{cm^2}$. By reducing porosity and permeability, microchannels have better thermal performance, the Nusselt number increases. In fact, the reduction of permeability from $K = 10^{-7}$ m^2 to $K = 10^{-9}$ m^2 results in an augment of 13 % in the average Nusselt number, while by reduction of porosity from $\varepsilon = 0.6$ to $\varepsilon = 0.4$ the average Nusselt number increases by 7%. This is because the reduction of these porous characteristics results in more moving of the hot fluid inside the porous medium toward the cold fluid of the clear region, which means better convective heat transfer of the coolant. Also, declining porosity and permeability ends up in a higher velocity in the clear region, and consequently a more exchanging of the momentum and energy fluxes. By looking more carefully, it can be also concluded that permeability has more

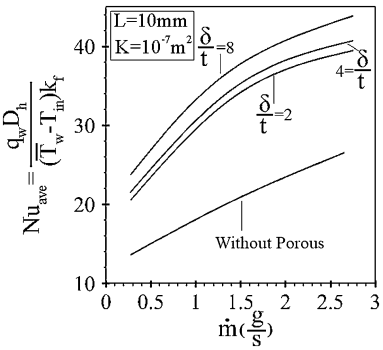

Figure 13. Variation of the average Nusselt number Nu_{ave} versus the mass flow rate for different porous layer thicknesses and the microchannel without porous medium.

impact on the average Nusselt number of microchannels compared to porosity.

The effect of mass flow rate $\dot{m}$ on the average Nusselt number Nu_{ave} for the microchannel with various porous layer thicknesses is represented in figure 13 Porosity is $\varepsilon = 0.6$ and permeability is $K = 10^{-7}m^2$. The average Nusselt numbers of microchannel without porous medium versus the mass flow rate is also shown. By increasing the mass flow rate, the average Nusselt number for both of the microchannel with and without porous medium increases; and the rate of this increase is larger for the microchannel with porous medium. For the microchannel with porous medium, the average Nusselt number increases more rapidly at lower mass flow rates compared to the higher mass flow rates. It can be also discerned that at larger porous layer thickness, the average Nusselt number escalate with the increase of $\dot{m}$ in a higher rate compared to smaller porous layer thicknesses.

5. Conclusion

Forced convection laminar flow and heat transfer has been numerically studied in a partially filled porous microchannel. The effect of porous layer thickness, permeability, porosity and mass flow rate are studied with using Darcy-Brinkman-Forchheimer equation for transport through the porous medium. For porous characteristics of $K = 10^{-7}$ and $\varepsilon = 0.6$, the microchannel with porous layer thicknesses of $\frac{\delta}{t}$ = 2, 4, 6, 8 and 10 have the pressure drop of 1.47, 1.78, 2.11, 2.49, and 2.93 times greater than the microchannel without porous medium. Simultaneously, they have Nusselt number of 1.64, 1.69, 1.75, 1.82 and 1.9 greater than the microchannel without porous medium. In addition, the decrease of porous characteristics of porosity and permeability leads to an increase in the fluid velocity of clear region, and at the same time, decrease of the fluid velocity in the porous region, which results in higher values for the Nusselt numbers and pressure gradients. By increasing of the mass flow rate, the average Nusselt number and pressure drop of microchannel with and without porous medium increase, and the rate of these increases is more rapidly for the microchannel with porous medium.

List of symbols

C	Forchheimer's constant
c_{pf}	Specific heat capacity at constant pressure of the fluid (J kg^{-1} K^{-1})
c_s	Specific heat capacity of solid (J kg^{-1} K^{-1})
D_h	Hydraulic diameter of the channel (m)
f	Friction factor
H	Height (m)
k	Thermal conductivity (W m^{-1} K^{-1})
K	Permeability of the porous medium (m^2)
L	Length (m)
Nu	Nusselt number
p	Pressure (Pa)
q_w	Heat flux on the bottom surface of the microchannel (W m^{-2})
T	Temperature (K)
t	Thickness of solid walls
u	Velocity component in x direction (m s^{-1})
u_{in}	Inlet velocity of the coolant (m s^{-1})
v	Velocity component in y direction (m s^{-1})
$\vec{V}$	Velocity vector (m s^{-1})
w	Velocity component in z direction (m s^{-1})
W	Width (m)
x	X coordinate
y	Y coordinate
z	z Coordinate

Greek letters

ε	Porosity
μ	Dynamic viscosity (kg m^{-1} s^{-1})
ρ	Density (kg m^{-3})
δ	Thickness of porous layer(m)
α	Aspect ratio

Subscripts

ave	Average
e	Effective property of the porous medium
f	Fluid
fd	Fully developed
in	Inlet
out	Outlet
s	Solid
W	Wall

References

[1] Adham A M, Mohd-Ghazali N and Ahmad R 2013 Thermal and hydrodynamic analysis of microchannel heat sinks: a review. *Renew. Sust. Energ. Rev.* 21: 614–622

[2] Tuckerman D and Pease R 1981 High-performance heat sinking for VLSI. *IEEE Electron. Device Lett.* 2: 126–129
[3] Kang Y and Chang J 2018 Channels in a porous scaffold: a new player for vascularization. *PFM* 13: 705–715
[4] Boland S and Majidi S 2021 Thermal improvement in double-layered microchannel heat sink with incorporating wavy porous fins. *Heat Transf. Eng.* 43: 458–502
[5] Jiang P, Wang Z, Ren Z and Wang B 1997 Forced convective heat transfer in a porous plate channel. *J. Therm. Sci.* 6: 43–53
[6] Ko K H and Anand N 2003 Use of porous baffles to enhance heat transfer in a rectangular channel. *Int. J. Heat Mass Transf.* 46: 4191–4199
[7] Zehforoosh A and Hossainpour S 2010 Numerical investigation of pressure drop reduction without surrendering heat transfer enhancement in partially porous channel. *Int. J. Therm. Sci.* 49: 1649–1662
[8] Chikh S, Boumedien A, Bouhadef K and Lauriat G 1998 Analysis of fluid flow and heat transfer in a channel with intermittent heated porous blocks. *Heat Mass Transf* 33: 405–413
[9] Deng B, Qiu Y and Kim C N 2010 An improved porous medium model for microchannel heat sinks. *Appl. Therm. Eng.* 30: 2512–2517
[10] Zhao C and Lu T 2002 Analysis of microchannel heat sinks for electronics cooling. *Int. J. Heat Mass Transf.* 45: 4857–4869
[11] Calmidi V V and Mahajan R L 2000 Forced convection in high porosity metal foams. *J. Heat Transfer* 122: 557–565
[12] Chen C H 2007 Forced convection heat transfer in microchannel heat sinks. *Int. J. Heat Mass Transf.* 50: 2182–2189
[13] Hetsroni G, Gurevich M and Rozenblit R 2006 Sintered porous medium heat sink for cooling of high-power mini-devices. *Int. J. Heat Fluid Flow* 27: 259–266
[14] Lu G, Zhao J, Lin L, Wang X D and Yan W M 2017 A new scheme for reducing pressure drop and thermal resistance simultaneously in microchannel heat sinks with wavy porous fins. *Int. J. Heat Mass Transf.* 111: 1071–1078
[15] Xu H 2020 Thermal transport in microchannels partially filled with micro-porous media involving flow inertia, flow/thermal slips, thermal non-equilibrium and thermal asymmetry. *Int. Commun. Heat Mass Transf.* 110: 1044404
[16] Huang P C and Vafai K 1994 Analysis of forced convection enhancement in a channel using porous blocks. *J. Thermophys. Heat Trans.* 8: 563–573
[17] Huang P and Vafai K 1993 Flow and heat transfer control over an external surface using a porous block array arrangement. *Int. J. Heat Mass Transf.* 36: 4019–4032
[18] Elsafy K M and Saghir M Z 2021 Forced convection in wavy microchannels porous media using TiO_2 and $Al2O_3$–Cu nanoparticles in water base fluids: numerical results. *Micromachines*12: 654
[19] Chuan L, Wang X D, Wang T H and Yan W M 2015 Fluid flow and heat transfer in microchannel heat sink based on porous fin design concept. *Int. Commun. Heat Mass Transf.* 65: 52–57
[20] Kozhukhov N, Kozhukhova E and Dubanin V 2018 Research on the hydrodynamics of coolant flow in compact heat exchangers filled with an inhomogeneous porous medium. In: *International Multi-Conference on Industrial Engineering and Modern Technologies (FarEastCon),* Vladivostok, Russia, pp. 1–6
[21] Aghamiri H, Niknejadi M and Toghraie D 2021 Analysis of the forced convection of two-phase Ferro-nanofluid flow in a completely porous microchannel containing rotating cylinders. *Sci. Rep.* 11: 17811
[22] Wang K and Li P 2018 Forced convection in bidisperse porous media incorporating viscous dissipation. *Appl. Therm. Eng.* 140: 86–94
[23] Li P, Zhang J, Wang K and Xu Z 2019 Heat transfer characteristics of thermally developing forced convection in a porous circular tube with asymmetric entrance temperature under LTNE condition. *Appl. Therm. Eng.* 154: 326–331
[24] Xu Z and Gong Q 2018 Numerical investigation on forced convection of tubes partially filled with composite metal foams under local thermal non-equilibrium condition. *Int. J. Therm. Sci.* 133: 1–12
[25] Baragh S, Shokouhmand H, Ajarostaghi S S M and Nikian M 2018 An experimental investigation on forced convection heat transfer of single-phase flow in a channel with different arrangements of porous media. *Int. J. Therm. Sci.* 134: 370–379
[26] Barnoon P and Toghraie D 2018 Numerical investigation of laminar flow and heat transfer of non-Newtonian nanofluid within a porous medium. *Powder Technol.* 325: 78–91
[27] Shen B, Yan H, Sunden B, Xue H and Xie G 2017 Forced convection and heat transfer of water-cooled microchannel heat sinks with various structured metal foams. *Int. J. Heat Mass Transf.* 113: 1043–1053
[28] Sheremet M A and Trifonova T A 2013 Unsteady conjugate natural convection in a vertical cylinder partially filled with a porous medium. *Numer. Heat. Tr. A-Appl.* 64: 994–1015
[29] Larimi Y M 2015 Constant wall heat flux boundary condition in micro-channels filled with a porous medium with internal heat generation under local thermal non-equilibrium condition. *Int. J. Heat Mass Transf.* 85: 524–542
[30] Hung T C, Huang Y X and Yan W M 2013 Thermal performance analysis of porous-microchannel heat sinks with different configuration designs. *Int. J. Heat Mass Transf.* 66: 235–243
[31] Yang Y T and Hwang C Z 2003 Calculation of turbulent flow and heat transfer in a porous-baffled channel. *Int. J. Heat Mass Transf.* 45: 771–780
[32] Vafai K and Sozen M 1990 Analysis of energy and momentum transport for fluid flow through a porous bed. *J. Heat Transfer* 112: 690–699
[33] Vafai K and Thiyagaraja R 1987 Analysis of flow and heat transfer at the interface region of a porous medium. *Int. J. Heat Mass Transf.* 30: 1391–1405
[34] Vafai K 2015 Handbook of Porous Media. 3rd edn. CRC Press, Florida
[35] Comsol Software 2020 Reference Manual, COMSOL Multiphysics version 5.6. Stockholm, Sweden, COMSOL LAB
[36] Beavers G S and Joseph D D 1967 Boundary conditions at a naturally permeable wall. *J. Fluid Mech.* 30: 197–207
[37] Cimolin F and Discacciati M 2013 Navier-Stokes/Forchheimer models for filtration through porous media. *Appl. Numer. Math.* 72: 205–224

[38] Alazmi B and Vafai K 2001 Analysis of fluid flow and heat transfer interfacial conditions between a porous medium and a fluid layer. *Int. J. Heat Mass Transf.* 44: 1735–1749

[39] Lori M S and Vafai K 2022 Heat transfer and fluid flow analysis of microchannel heat sinks with periodic vertical porous ribs. *Appl. Therm. Eng.* 205: 118059

[40] Ghahremannezhad A and Vafai K 2018 Thermal and hydraulic performance enhancement of microchannel heat sinks utilizing porous substrates. *Int. J. Heat Mass Transf.* 122: 1313–1326

[41] Yen Y L, Huang P C, Yang C F and Chen Y J 2008 Numerical study of heat transfer of a porous-block-mounted heat source subjected to pulsating channel flow. *Numer Heat Tr. A-Appl.* 54: 426–449

[42] Hadim A 1994 Forced convection in a porous channel with localized heat sources. *ASME. J. Heat Transfer.* 116: 465–472

[43] Worster M G 1997 Convection in mushy layers. *Annu. Rev. Fluid Mech.* 29: 91–122

[44] Worster M G 2000 Solidification of fluids. Cambridge University Press, Cambridge

[45] Levy T and Sanchez-Palencia E 1974 On boundary conditions for fluid flow in porous media. *Int. J. Eng. Sci.* 13: 923–940

[46] Schulze T P and Worster M G 1999 Weak convection, liquid inclusions and the formation of chimneys in mushy layers. *J. Fluid Mech.* 388: 197–215

[47] Ochoa-Tapia J and Whitaker S 1995 Momentum transfer at the boundary between a porous medium and a homogeneous fluid—I. Theoretical development. *Int. J. Heat Mass Transf.* 38: 2635–2646

[48] Ochoa-Tapia J and Whitaker S 1995 Momentum transfer at the boundary between a porous medium and a homogeneous fluid—II. Comparison with experiment. *Int. J. Heat Mass Transf.* 38: 2647–2655

[49] Neale G H and Nader W K 1974 Prediction of transport processes within porous media: creeping flow relative to a fixed swarm of spherical particles. *AIChE Journal* 20: 530–538

[50] Cieszko M and Kubik J 1999 Derivation of matching conditions at the contact surface between fluid-saturated porous solid and bulk fluid. *Transp Porous Media* 34: 319–336

[51] Lori M and Vafai K 2022 Thermal and hydraulic performance of rectangular microchannel heat sinks with trapezoidal porous configuration. *Numer. Heat Tr. A-Appl.* 81: 72–93

[52] Shah R and London A 1973 Laminar Flow forced convection in ducts. Academic Press, New York

[53] Jung J Y and Kwak H Y 2008 Fluid flow and heat transfer in microchannels with rectangular cross section. *Heat Mass Transf.* 44: 1041–1049

[54] Ma H, Duan Z, Ning X and Su L 2021 Numerical investigation on heat transfer behavior of thermally developing flow inside rectangular microchannels. *Case Stud. Therm. Eng.* 24: 100856

[55] Montgomery S and Wibulswas P 1968 Laminar flow heat transfer for simultaneously developing velocity and temperature profiles in ducts of rectangular cross section. *Appl. Sci. Res.* 18: 247–259